International Refrigeration and Air Conditioning Conference   School of Mechanical Engineering

2021

Condensation Heat Transfer of R410A Inside Multiport Minichannels with Different Cross-sectional Geometry

Hoang Ngoc Hieu
Chonnam National University

Nurlaily Agustiarini
Chonnam National University

Pham Quang Vu
Electric Power University Hanoi

Jong-Taek Oh
Chonnam National University

CONDENSATION HEAT TRANSFER OF R410A INSIDE MULTIPORT MINICHANNELS WITH DIFFERENT CROSS-SECTIONAL GEOMETRIES

Hieu Ngoc HOANG[1], *Nurlaily* AGUSTIARINI[1], Vu Quang PHAM[2], Jong-Taek OH[3]*

[1]Department of Refrigeration and Air-Conditioning, Graduate School, Chonnam National University
Yeosu, 59626 Chonnam, Korea

[2]Faculty of Energy Technology, Electric Power University
Hanoi, Vietnam

[3]Department of Refrigeration and Air-Conditioning, Chonnam National University
Yeosu, 59626 Chonnam, Korea
ohjt@chonnam.ac.kr

* Corresponding Author

ABSTRACT

Condensation heat transfer of R410a in a multiport mini-channels tubes with different cross-sectional geometry is experimentally investigated. Three tubes with aspect ratio of 0.395, 0.385 and 0.446, and hydraulic diameters of 1.147 mm, 1.135 mm and 0.846 mm with number of channels (7, 11 and 18) are tested in this study. The experimented range of heat flux is from 3 to 15 kW/m2, mass flux from 50 to 500 kg/m^{2}s. The data show that the heat transfer coefficient increases with heat flux, mass flux and vapor quality. A performance comparison was conducted among the 3 tested tubes and it was found out that the number of channels increases heat transfer coefficient significantly at low heat flux and mass flux, while this effect is damped at higher heat/mass flux condition. In addition, it was found that heat transfer in small hydraulic diameter and high aspect ratio channels deteriorated. Possible mechanism to this deterioration is proposed. Finally, a new correlation is developed to predict the heat transfer coefficient of R410a in a multiport mini-channels tube.

1. INTRODUCTION

Mini and microscale heat transfer technology has been widely adopted in recent years. Their chief advantages over conventional size instruments including reduced weight, material cost, refrigerant charge while still retaining an adequately high heat transfer rate. Therefore, further studies should be conducted to not only advance understanding of miniature condensation phenomena but also to maximize their efficiency in practical application.

In recent years, significant number of papers has been dedicated to different technical aspects of the technology. Sakamatapan et al (2013) studied the condensation heat transfer characteristic of R134a inside two multiport mini-channels with the hydraulic diameter 1.1 and 1.2 and aspect ratio successively of 1.25 and 0.5. Their data mostly fall onto the annular flow and mist flow regimes when plotted on the map of Coleman and Garimella (1999). They found that mass flux and vapor quality increase the heat transfer coefficient. As for the geometrical effect, it was observed that the smaller hydraulic diameter yields a higher heat transfer coefficient.

Liu et al (2016) conducted an experimental investigation of heat transfer and pressure drop of three refrigerants: R290, R1234ze and R22 in a circular tube of 1.085 mm diameter and a square channel of 0.952 mm. Similar trend is reported, that heat transfer coefficient increases with vapor quality, heat flux and mass flux and decreases with saturated temperature for all 3 refrigerants. Heat transfer coefficient of propane is larger than that of R1234ze(E) which is then larger than those of R22. On the effect of channel geometry, they found that the square channel's heat transfer coefficient is larger than the circular channel at the same experimental condition.
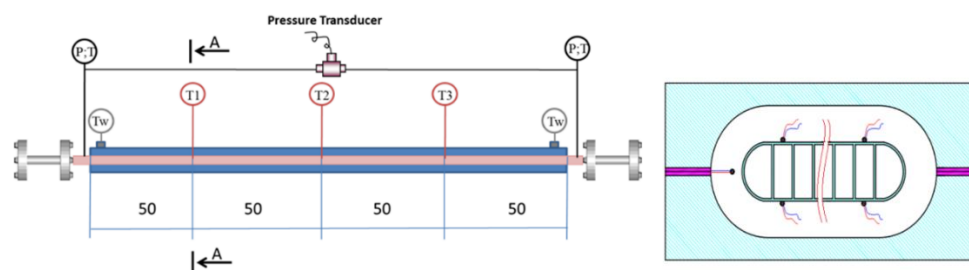
Similar to Liu, Shin & Kim (2005) experimentally studied flow condensation of R134a for a single circular channel of 0.493mm, 0.619mm, 1.067mm and square channel of 0.494mm, 0.658mm, 0.972mm hydraulic diameter. Their report is similar to Liu et al (2016) except that they did not find a clear relationship between heat flux and heat transfer coefficient. On the effect of cross-sectional geometry, clear enhancement of heat transfer is found with decreasing hydraulic diameter. For low mass flux, the rectangular channel has a higher heat transfer coefficient, while the reverse is true at higher mass flux. They attributed this result to the effect of surface tension at the corners, similar to Liu's explanation.

The pressure drop and heat transfer coefficient of 4 different refrigerants: R32. R134a, R1234ze(E) and R410a in rectangular multiport mini-channels of 0.85 hydraulic diameter is investigated (2016) by Jige et al. A common trend of increasing heat transfer with mass flux and vapor quality is observed again. They found that the heat transfer coefficient for R32 is higher than that of R1234ze due to the higher thermal conductivity of R32. They also compared their data with Nakashita's data (2002) of multiport mini-channels with diameters of 0.79 and 1.06 and found out that heat transfer increases with decrease in hydraulic diameter, although the effect of diameter is weaker at high heat flux. It should be noted that channels in comparison all have different aspect ratios.

Although a significant number of papers devoted to the study of mini/micro scale condensation heat transfer has been published recently, there still many open problems that need to be resolved. The effect of channel cross-sectional geometry on heat transfer still require an additional study. In this work, three channels consist of two channels with similar aspect ratio and hydraulic diameter, and one channel with a slightly higher aspect ratio and 25% smaller diameter are studied. R410a is chosen as the studied fluid because of its current wide usage and its role in the future as a substitution for the soon phased-out R-22. The resulting data with one unprecedented trend, will be presented. Subsequently, a new correlation for the prediction of heat transfer coefficient is proposed.

2. EXPERIMENTAL APPARATUS

The schematic diagram of the experimental apparatus for this study is presented in Figure 1. The experimental set-up is composed of a refrigeration loop, a chilled water loop and a data acquisition system.

Figure 1: Experimental apparatus

Refrigerant is circulated by a magnetic gear pump coupled with inverter for adjusting the mass flux. Vapor is generated inside the preheater with DC power. In the inlet, the vapor quality of the test section is controlled by varying the DC power supply at the preheater. Mass flow rate is measured with a Coriolis type flow meter installed after the sub-cooler. Saturated vapor is then partially condensed inside the test section and then condensed completely inside the condenser, both with chilled water. Two sight glasses are installed at the inlet and outlet of the test section to serve the flow visualization purpose. Liquid refrigerant post condenser is received before being recirculated with the gear pump. The experimental apparatus system is well-insulated to minimize heat loss affecting the testing procedure. Chilled water is supplied by a chiller unit with pump circulation. Water mass flow rate is measured with a flow meter for the calculation of the applied heat flux to the test section in the data reduction section.

Figure 2: Test section and cross-sectional area in detail

The detail of the test section and the cross-sectional detail are shown in figure 2. Test section is designed as a counter-current, tube in tube heat exchanger with refrigerant condensing flow in the inner channel and chilled water flow in the outer annulus cover made of acrylic. Geometric parameters of the testing multiport mini-channels are shown in table 1. In order to calculate the heat transfer coefficient, temperature of the outer wall of the test section is measured with 12 0.13mm K-type thermocouples. The thermocouples are attached as shown in the figure, with 2 attached on the top side and 2 on the bottom side. Four resistance temperature sensors were used to measure inlet and outlet temperature of the refrigerant and the cooling water. For the measurement of pressure drop, a differential pressure transducer is installed at the inlet and outlet of the mini-channels. Saturated pressure is monitored with an absolute pressure sensor.

Table 1: Test section detailed geometrical configuration

Channels	H (mm)	W (mm)	d_h (mm)	β=W/H	n	D (mm)	L (m)
A	2	0.79	1.147	0.395	7	0.25	0.2
B	2	0.77	1.135	0.385	11	0.25	0.2
C	1.3	0.58	0.846	0.446	18	0.25	0.2

Table 2: Experimental conditions

Refrigerant	q (kW/m²K)	G (kg/m²s)	T_{sat}
R410a	3 - 15	50 – 500	48

3. DATA REDUCTION METHOD

The test section inlet vapor quality is controlled by DC power supplied, through heat-balance at the preheater the inlet quality can be calculated as:

$$x_{in} = \frac{1}{h_{fg}}\left[\frac{Q_{pre-heater}}{m_{ref}} - C_p(T_s - T_{inlet})\right] \tag{1}$$

The test section average heat flux is determined from the inlet and outlet chilled water temperature differences:

$$q = \frac{m_{water}\, C_{p,water}\, \Delta T_{water}}{A_{external}} \tag{2}$$

Also with heat balancing, the test section's outlet vapor quality can be calculated by:

$$x = x_{inlet} - \frac{m_{water}\, C_{p,water}\, \Delta T_{water}}{2 m_{ref} h_{lg}} \tag{3}$$

One-dimensional steady state heat conduction is assumed between the inner and outer wall of the channel. The inner wall temperature can be calculated by: Condensation Heat Transfer of R410A inside Multiport Mini-channels with Different Cross-sectional Geometries

$$T_{w,i} = T_{w,o} \frac{q \delta_{aluminium}}{k_{aluminium}} \tag{4}$$

With the channel's inner temperature, the heat transfer coefficient can be obtained. The differences between the internal and external heat transfer area are also considered,

$$h = \frac{A_{external}}{A_{internal}} \frac{q}{(T_{sat}-T_{w,i})} \tag{5}$$

In this study, the experimental uncertainty analysis has been performed in agreement with the guidelines provided by ISO (1995).

Table 3: Uncertainty of measurement and calculation

Parameters	Uncertainty
Temperature	±0.1K
Absolute pressure	±2.5kPa
Mass flux	±0.5%
Heat flux	±3%
Vapor quality	±5%
Heat transfer coefficient	±11.7%

4. RESULT AND DISCUSSION

4.1 The effect of mass flux, heat flux and vapor quality

In this section, the effect of mass flux, heat flux and vapor quality on the heat transfer coefficient is discussed through the experimental results.

In figure 3, heat transfer coefficient data is plotted against mass quality for different mass flux values ranging from 50 kg/m²s to 500 kg/m²s at the same heat flux 6 kW/m²K. Here it can be seen from the graph that heat transfer coefficient increases with mass flux and vapor quality. According to Coleman and Garimella (1999), at high vapor quality, the dominant flow pattern for miniature size channels (roughly 1mm or below) is annular flow regime. In annular flow regime, the liquid film is thinner at high quality and thicker at lower quality. Therefore, as condensation proceeds, the thermal resistance of the film will increase with its thickness, and hence decrease the overall heat transfer coefficient. The effect of mass flux on the heat transfer can be attributed to two distinct mechanisms. First, increasing the mass flux increases the vapor velocity, which in turn increases the relative velocities between the two phases and subsequently, the shear stress at the interface. Secondly, higher mass flux allows for stronger turbulence effect, which corresponds to higher Reynolds number. This increment in convection as well as in interfacial shear together enhance the heat transfer.
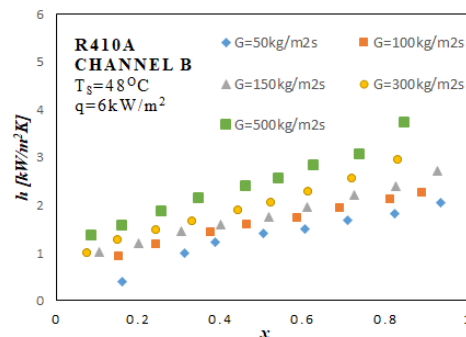

Figure 3: The effect of mass flux on heat transfer coefficient

Figure 4 plotted heat transfer coefficient against mass quality at the same mass flux of 300 kg/m²s and heat flux range from 3 to 15 kW. The graph also shows that heat transfer coefficient increases with heat flux. The effect is stronger at the lower heat flux range from 3 to 9 and weaker from 9 to 15. Authors suggest the increase in heat flux increases the level of liquid sub-cooling, which in turn enhances both the heat and mass transport within the flow. Sakamatapan suggested that heat flux could affect flow mechanics and lead to better heat transfer.
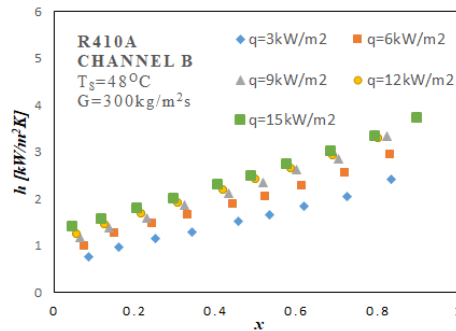
Figure 4: The effect of heat flux on heat transfer coefficient

4.2 The effect of channel's geometry

In figure 5, heat transfer coefficient is plotted against mass quality at the same heat flux and mass flux condition but for different channels.
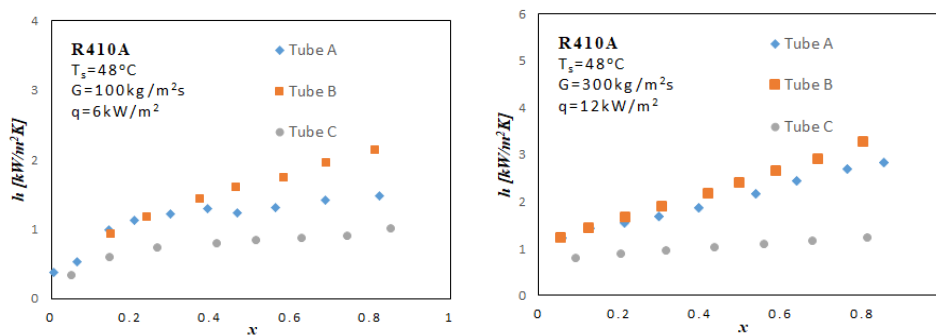
Figure 5: Heat transfer coefficient of tube A,B and C at low and high heat flux, mass flux condition

From table 1, tube A and B have similar hydraulic diameter and aspect ratio, the only difference is in the number of channels inside the tube (7 and 11 channels respectively). The results show the impact of the number of channels has on the heat transfer coefficient. At lower heat flux and mass quality, the effect of the number of channels is more dominant. Especially at high quality, heat transfer coefficient could increase up to 46% maximum and about 30% on average. At high mass flux and high heat flux however, the effect of the number of channel on heat transfer is more difficult to notice. Yun et al attributed this increase to the more even distribution of heat flux among the channels of the tube.

The effect of hydraulic diameter is also evident from the two graphs. The results show that for both higher and lower mass flux and vapor quality, decreasing the hydraulic diameter decreases heat transfer coefficient, which is in contrary to the trends often found in literature. In the analysis in the correlation development section, it is shown from equation (8), decreasing the hydraulic diameter will lead to a reduction in Reynolds number, which will therefore negatively affect the impact of turbulence and interfacial shear stress on heat transfer. It is speculated that in channel with extreme value (high or small) of the aspect ratio, the effect of no-slip wall condition and flow confinement might suppress mixing and turbulence and reduce overall heat transfer. However, this effect is not yet clearly understood and should be a topic of future study.

4.3 Comparison with existing correlations

Experimental data were compared against 6 existing heat transfer correlations available in literature: which are correlations proposed by Koyama et al. (2003), Rahman et al (2018), Shah et al, Jige et al (2016), Kim et al (2013).

and by Pham (2019). The performance of these six correlations is graphed in figure 6 while the value mean deviation and average deviation are presented in Table 4.

The performance of the existing correlation will be evaluated by mean and average deviation which is calculated as follow

$$AD = \frac{1}{n_{data}} \sum_{1}^{n_{data}} 100\% \frac{h_{predict} - h_{experimental}}{h_{experimental}} \qquad (6)$$

$$MD = \frac{1}{n_{data}} \sum_{1}^{n_{data}} 100\% \frac{|h_{predict} - h_{experimental}|}{h_{experimental}} \qquad (7)$$
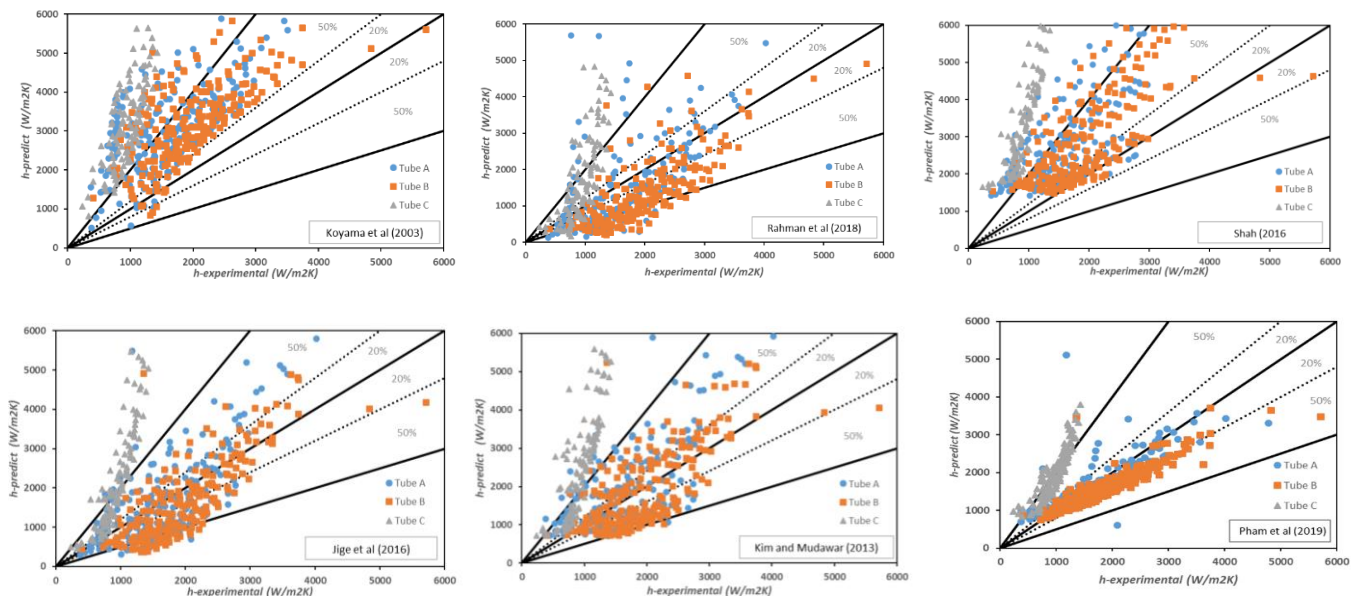
Figure 6: Comparing the existing correlation against experimental data

Table 4: Correlation's Mean and Average deviation

		Koyama	Rahman	Shah	Jige	Kim	Pham
MD	**Tube A**	*109.0%*	*64.3%*	*90.2%*	*38.3%*	*44.6%*	*24.6%*
	Tube B	*72.3%*	*41.8%*	*56.2%*	*31.1%*	*31.6%*	*32.7%*
	Tube C	*244.5%*	*94.8%*	*287.9%*	*125.0%*	*172.0%*	*68.9%*
	All	*123.3%*	*61.8%*	*118.8%*	*54.0%*	*66.6%*	*37.3%*
AD	**Tube A**	*108.0%*	*5.6%*	*89.6%*	*3.1%*	*24.1%*	*-10.5%*
	Tube B	*71.1%*	*-34.4%*	*55.1%*	*-16.9%*	*0.4%*	*-31.0%*
	Tube C	*244.5%*	*82.0%*	*287.9%*	*125.0%*	*172.0%*	*68.9%*
	All	*122.4%*	*5.9%*	*118.2%*	*21.2%*	*46.3%*	*-1.7%*

From the figure and the table, it is seen that none correlation made a satisfying prediction against the experimental data. Especially for the data of tube C, all correlation severely overpredict the experimental data up to 287%. Indeed, this implies that a new correlation is needed to make a more accurate prediction for observation.

5. NEW CORRELATION

In this study, a new correlation is developed based on the modelling method proposed by Jige et al (2016). Here, only annular and intermittent flow regime (namely slug flow) will be analyzed with simplified model. Effect that has not been included in the model will be introduced by curve-fitting experimental data.

5.1 Annular flow heat transfer model

The following modelling and analysis follow the Jige's paper of 2016, in which he proposed a film condensation model (8), comprising two terms which represent the vapor shear dominated case (1st term of equation 8) and surface tension dominated cases (2nd term of equation 8). Both cases will be analyzed separately.

$$\frac{\mu_l k_l (T_s - T_w) t^2}{8\rho_l \delta \Delta h} = \frac{t^2}{16} \frac{\partial}{\partial z} \left(\frac{\tau_i \delta^2}{2}\right) + \frac{\delta^3}{3} \frac{\sigma}{r_c} \tag{8}$$

5.2 Vapor shear stress dominated case
For cases where the mass flux is high, the surface tension effect is expected to be small and therefore its term is neglected in equation (8). The length z can be replaced through relation with heat flux obtained from heat balance. For the interfacial shear stress, Jige's equation will be used. Finally, we include a curve-fitting term of high mass flux data to consider the turbulence effect in film flow. The shear dominated Nusselt number is formulated as

$$Nu_{an,shear} = \left(0.323 + 0.07 Re_l^{0.313} Pr_l^{0.6267}\right) \frac{\Phi_v}{1-x} \sqrt{f_{vo} \frac{\rho_l}{\rho_v} Re_l \left(\frac{n\beta + (n-1)\eta_{fin} + 1}{n(\beta+1)}\right)} \tag{9}$$

The two-phase frictional multiplier and the friction factors for vapor and liquid phases that appeared in equation (9) are given also provided in Jige (2016). Their equation will be included in the table 6.

5.3 Surface tension dominated case
For flow with low mass flux, shear stress term in (8) will be neglected, then surface tension dominated annular flow Nusselt number can be formulated. It is speculated that the channel aspect ratio will an important parameter for surface tension dominated flow. The Nusselt number for this case is then formulated as:

$$Nu_{an,st} = 0.0047\beta^{-6.62} \left[\frac{\rho_l \Delta h \sigma d_h}{k_l \mu_l (T_s - T_w)}\right]^{0.25} \tag{10}$$

5.5 Annular flow Nusselt number
The final annular flow Nusselt number combined the effect of interfacial shear and surface tension by super-positioning these two terms. Two new factors taking into account the suppression or enhancement F_{shear} and F_{st} of each effect are included in the equation. They are expected to be functions of We_l and the dimensionless number $(q/G\Delta h)$. Curve-fitting the data for F_{shear} and F_{st}, annular flow Nusselt number can be found as:

$$Nu_{an} = 0.0008 We_l^{0.0744} \left(q/_{G\Delta h}\right)^{-0.5344} Nu_{an,shear} + 133.37 We_l^{0.32} \left(q/_{G\Delta h}\right)^{0.66} Nu_{an,st} \tag{11}$$

5.4 Slug flow modeling
Slug flow is modelled as a continuously alternating flow of single-phase liquid and two-phase annular film flow. Thus, vapor plug Nusselt number is considered to be equal to annular flow Nusselt number and liquid slug Nusselt number can then be calculated with well-known existing correlationsfor single phase liquid flow by Gnielinski (1976) and Hartnett, Kostic (1989).
The slug flow regime Nusselt number can be expressed by time-averaging the Nusselt number of vapor slug and liquid slug regime. The following equation are given from Jige's analysis.

$$Nu_{slug} = Nu_{an}\alpha + (1-\alpha)Nu_{ls} \tag{12}$$

5.5 Condensation heat transfer correlation
The final condensation heat transfer correlation is assembled by combining all effect of both slug and annular flow regime that was previously discussed. The functional form is given as as similarly in Jige and is summarized in the bellow table

Table 6: Correlation Summarization

$Nu = Nu_{an}\alpha + (1-\alpha)Nu_{ls},\ Nu_{an} = 0.0008 We_l^{0.0744}\left(q/_{G\Delta h}\right)^{-0.5344} Nu_{an,shear} + 133.37 We_l^{0.32}\left(q/_{G\Delta h}\right)^{0.66} Nu_{an,st}$
$Nu_{an,shear} = \left(0.323 + 0.07 Re_l^{0.313} Pr_l^{0.6267}\right)\frac{\Phi_v}{1-x}\sqrt{f_{vo}\frac{\rho_l}{\rho_v}Re_l\left(\frac{n\beta+(n-1)\eta_{fin}+1}{n(\beta+1)}\right)},\ Nu_{an,st} = 0.0047\beta^{-6.62}\left[\frac{\rho_l\Delta h\sigma d_h}{k_l\mu_l(T_s-T_w)}\right]^{0.25}.$
$\Phi_v^2 = x^{1.8} + (1-x)^{1.8}\frac{\rho_l f_{lo}}{\rho_v f_{vo}} + 0.65 x^{0.68}(1-x)^{0.43}\left(\frac{\mu_l}{\mu_v}\right)^{1.25}\left(\frac{\rho_l}{\rho_v}\right)^{0.75}$
$f_{vo} = \begin{cases} C_1/\left(Gd_h/_{\mu_v}\right) & for\ \left(Gd_h/_{\mu_v}\right) \le 1500 \\ 0.046/\left(Gd_h/_{\mu_v}\right)^{0.2} & for\ \left(Gd_h/_{\mu_v}\right) > 1500 \end{cases},\ f_{vo} = \begin{cases} C_1/\left(Gd_h/_{\mu_l}\right) & for\ \left(Gd_h/_{\mu_v}\right) \le 1500 \\ 0.046/\left(Gd_h/_{\mu_v}\right)^{0.2} & for\ \left(Gd_h/_{\mu_v}\right) > 1500 \end{cases},\ \alpha = \frac{x}{x+(1-x)^{\rho_v}/_{\rho_l}}$

$$Re_l = \frac{G(1-x)d_h}{\mu_l}, \ We = \frac{G^2 d_h}{\rho_l \sigma}, \ Pr_l = \frac{\mu_l c_{pl}}{k_l}, Nu = \frac{h d_h}{k_l}$$

$$\eta = \frac{2(e^{mH} - e^{-mH})(1 - e^{-mH})(e^{mH} - 1)}{mH}, \ m = \sqrt{\frac{2h}{W_{fin} k_{fin}}}.$$

5.6 Correlation performance

Figure 7 show the performance of the new correlation against experimental data from this study, and table 5 show the average and mean deviation of the correlation. Comparing with existing correlations in literature, it is evidence that the new correlation prediction is more accurate, with the smallest value of mean deviation and the highest number of points falling into the 20% and 50% error bands (81% and 97.3% respectively).
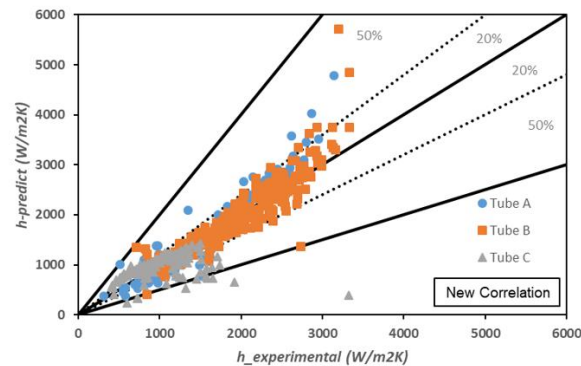

Figure 7: Comparing the new correlation against experimental data

Table 5: New correlation's AD and MD

MD				AD			
Tube A	Tube B	Tube C	All	Tube A	Tube B	Tube C	All
12.3%	*10.7%*	*21.2%*	*13.6%*	*2.5%*	*2.1%*	*10.3%*	*4.1%*

6. CONCLUSIONS

In this work, condensation heat transfer coefficient of R410a in three multiport channels with different geometrical configuration is experimentally studied. Key findings are summarized as follows.

- Heat transfer coefficient increases with heat flux, mass flux and vapor quality, trends that are also reported from many previous papers.
- Both the number of channels inside the multiport tubes and hydraulic diameter are important to the heat transfer coefficient of the tube. The number of channel increases significantly the heat transfer coefficient at low heat flux, mass flux condition especially at high quality regions. Heat transfer coefficient is degraded in channels with small diameter and high aspect ratio, possibly due to the reduction of Reynolds number, although this effect is not yet fully understood.
- A new correlation is proposed, modifying from the original model of Jige (2016). The proposed correlation showed better agreement with measured heat transfer coefficient comparing to previously available correlations in literature.

NOMENCLATURE

A	Area	(m^2)	**Greeks**		
C$_p$	Specific Heat	(kJ/kg K)	α	Void fraction	
d$_h$	Hydraulic diameter	(m)	Δ	Difference	
D	Channel's thickness	(m)	δ	Liquid film thickness (m)	
H	channel's height	(m)	σ	Surface Tension (N/m)	
h	heat transfer coefficient	(W/m^{2}K)			

Δh	Latent heat of vaporization	(kJ/kg)	μ	Viscosity (Ns/m^2)
f	Frictional Factor		ρ	Density (kg/m^3)
G	Mass flux	(kg/m^2 s)	τ	Shear stress (N/m^2)
k	Thermal conductivity	(kW/mK)	β	Aspect ratio (=W/H)
L	Channel length	(m)	δ	Thickness (m)
$\dot{m}$	Mass flow rate	(kg/s)	ϕ	Two-phase frictional multiplier
m	Fin's parameter		**Subscripts**	
n	Number of channel		an	annular flow
Nu	Nusselt number		an,shear	annular flow, shear stress dominated
Pr	Prandtl number		an,st	annular flow, surface tension dominated
P	Pressure	(MPa)	crit	Critical
r_c	Radius of Curvature	(m)	exp	Experimental value
Q	Heat capacity	(kJ)	fin	fin
q	Heat flux	(kW/m^2)	l	Liquid
Re	Reynolds number		ls	liquid slug
T	Temperature	(K)	g	Vapor
t	Length of the condensate film region	(m)	i	Interfacial
			in	Inner
W	channel's width	(m)	o	Outer
We	Weber number		lo	Liquid only
x	Vapor quality		s	Saturation
z	Axial coordinate	(m)	vp	Vapor plug
			w	Wall

REFERENCES

Awad, M. M., Dalkilic, A. S., Wongwises, S. (2014), A Critical Review on Condensation Heat Transfer in Microchannels and Minichannels, J. Nanotechnol. Eng. Med., DOI: 10.1115/1.4028092

Cavallini, A., Censi, A., Del Col, Doretti, L., Longo, G., Rossetto, L. (2001), Experimental investigation on condensation heat transfer and pressure drop of new HFC refrigerants (R134a, R125, R32, R410A, R236ea) in a horizontal smooth tube, *Int. J. Refrigeration* 24 73±87

Cavallini, A., Doretti, L., Matkovic, M. & Rossetto, L., (2006) Update on Condensation Heat Transfer and Pressure Drop inside Minichannels, *Heat Transfer Engineering*, 27:4, 74-87, DOI: 10.1080/01457630500523907

Choi, I-H & Kim, N-H (2020): Flow condensation of R-410A in multiport tubes having smooth or micro-finned internal channels, *Experimental Heat Transfer*, DOI: 10.1080/08916152.2020.1826598

Chowdhury, S., Al-Hajri, E., Dessiatoun, S., Shooshtari, A., and Ohadi, M. (2006), "An Experimental Study of Condensation Heat Transfer and Pressure Drop in a Single High Aspect Ratio Micro-Channel for Refrigerant R134a," *Proceedings of the 4th International Conference on Nanochannels, Microchannels and Minichannels (ICNMM2006), Limerick, Ireland*, June 19-21, Vol. A, Paper No. ICNMM2006-96211, pp. 147-154.

Coleman, J.W., Garimella, S. (1999), Characterization of two-phase flow patterns in small diameter round and rectangular tubes, *Int. J. Heat Mass Transfer* 42, 2869-2881

Jige, D., Inoue, N., Koyama, S. (2016), Condensation of refrigerants in a multiport tube with rectangular minichannels, *Int. J. Refrigeration* ,http://dx.doi.org/doi: 10.1016/j.ijrefrig.2016.03.020.

Kim, N. H., Cho, J. P., Kim, J. O., Youn, B. (2003), Condensation heat transfer of R-22 and R-410A in flat aluminum multi-channel tubes with or without micro-fins, *Int. J. Refrig-Revue Internationale Du Froid* 26 830–839

Kim, S. M., Mudawar, I. (2013), Universal approach to predicting heat transfer coefficient for condensing mini/micro-channel flow, *Int. J. Heat Mass Transfer* 56, 238-250

Koyama, S., Kuwahara, K., Nakashita, K., Yamamoto, K. (2003), An experimental study on condensation of refrigerant R134a in a multi-port extruded tube, *Int. J. Refrigeration* 24 425–432

Liu, N., Xiao, H., Li, J. (2016), Experimental investigation of condensation heat transfer and pressure drop of propane, R1234ze(E) and R22 in minichannels, *Applied Thermal Engineering* 102, 63–72

López-Belchí, A., Illán-Gómez, F., Cascales, J. F. G, García, F. V. (2016), R32 and R410A condensation heat transfer coefficient and pressure drop within minichannel multiport tube. Experimental technique and measurements, *Applied Thermal Engineering*, doi: http://dx.doi.org/10.1016/j.applthermaleng.2016.05.143

Rahman, M. M, Kariya, K., Miyara, A. (2018), An experimental study and development of new correlation for condensation heat transfer coefficient of refrigerant inside a multiport minichannel with and without fins, *Int. J. Heat Mass Transfer* 116, 50–60

Sakamatapan, K., Kaew-On, K., Delkilic, A. S., Mahian, O., Wongwises, S. (2013), Condensation heat transfer characteristics of R-134a flowing inside the multiport minichannels, *Int. J. Heat Mass Transfer* 64, 976–985

Shah, M.M. (2016), A correlation for heat transfer during condensation in horizontal mini/micro channels, *Int. J. Refrigeration* ,http://dx.doi.org/doi: 10.1016/j.ijrefrig.2015.12.008.

Shin, J.S & Kim, M. H., (2005) An Experimental Study of Flow Condensation Heat Transfer Inside Circular and Rectangular Mini-Channels, *Heat Transfer Engineering*, 26:3, 36-44, DOI: 10.1080/01457630590907185

Vu, P.Q., Choi, K. I., & Oh J. T. (2019): Condensation Heat Transfer Characteristics and Pressure Drops of R410A, R22, R32, and R290 in Multiport Rectangular Channel, *Science and Technology for the Built Environment*, DOI:10.1080/23744731.2019.1665447

Yun, R., Heo, J. H., Kim, Y. (2006), Evaporative heat transfer and pressure drop of R410A in Microchannels, *Int. J. Refrigeration* 29, 92–100

Zhang, H-Y., Li, J. M, Liu, N., Wang, B-X. (2012), Experimental investigation of condensation heat transfer and pressure drop of R22, R410A and R407C in mini-tubes, *Int. J. Heat Mass Transfer.*, 55, 3522–3532

Nakashita, K. (2002), Study on condensation of pure refrigerant R134a in multi-port extruded tubes, Doctoral thesis; Kyushu University

ACKNOWLEDGEMENT